Estimating PV Power from Aggregate Power Measurements within the Distribution Grid

E. Vrettos,[1, a)] E. C. Kara,[2, b)] E. M. Stewart,[3, c)] and C. Roberts[4, d)]
[1)]*Grid Integration Group, Lawrence Berkeley National Laboratory, Berkeley, CA, USA*
[2)]*SLAC National Accelerator Laboratory, Menlo Park, CA, USA*
[3)]*Lawrence Livermore National Laboratory, Livermore, CA, USA*
[4)]*Electrical Engineering and Computer Science, University of California, Berkeley, CA, USA*

(Dated: 7 April 2019)

The increased integration of photovoltaic (PV) systems in distribution grids reduces visibility and situational awareness for utilities, because the PV systems' power production is usually not monitored by them. To address this problem, a method called Contextually Supervised Source Separation (CSSS) has been recently adapted for real-time estimation of aggregate PV active power generation from aggregate net active and reactive power measurements at a point in a radially configured distribution grid (e.g., substation). In its original version, PV disaggregation is formulated as an optimization problem that fits linear regression models for the aggregate PV active power generation and true substation active power load. This paper extends the previous work by adding regularization terms in the objective function to capture additional contextual information such as smoothness, by adding new constraints, by introducing new regressors such as ambient temperature, and by investigating the use of time-varying regressors. Furthermore, we perform extensive parametric analysis to inform tuning of the objective function weighting factors in a way that maximizes performance and robustness. The proposed PV disaggregation method can be applied to networks with either a single PV system (e.g., MW scale) or many distributed ones (e.g., residential scale) connected downstream of the substation. Simulation studies with real field recorded data show that the enhancements of the proposed method reduce disaggregation error by 58% in winter and 35% in summer compared with previous CSSS-based work. When compared against a commonly used transposition model based approach, the reduction in disaggregation error is more pronounced (78% reduction in winter and 45% in summer). Additional simulations indicate that the proposed algorithm is applicable also for PV systems with time-varying power factors. Overall, our results show that – with appropriate modeling and tuning – it is possible to accurately estimate the aggregated PV active power generation of a distribution feeder with minimal or no additional sensor deployment.

I. INTRODUCTION

As the penetration of distributed photovoltaic (PV) generation continues to increase in the distribution network, operators are facing new challenges in the management of active distribution networks. Distributed PV systems are typically not monitored in real-time, and large aggregations of these installations can result in large ramp rates and power swings in the net demand at the substation. This work seeks to alleviate the lack of visibility into the aggregated behavior of these systems in order to provide system operators with greater insight into the network behavior, and do so with minimal or no additional sensing and communication. In particular, we envisage that having accurate information on the aggregated active power generation of a feeder will result in better distributed PV generation forecasting given irradiance forecasts and, consequently, reduce the over-procurement of reserves (Palmintier *et al.*, 2016). Additionally, it can help system operators to intelligently re-tune regulation equipment to minimize voltage deviations, while also maximizing the expected lifetime of equipment (Mehmood *et al.*, 2018).

The goal of this work is to estimate (or disaggregate) the instantaneous *aggregated* PV active power generation of a distribution feeder or small geographic area. This is an alternative to recently proposed approaches that use smart meter measurements to infer the PV generation of *individual* residences, an extension of traditional non-intrusive load monitoring (Chen and Irwin, 2017; Kara *et al.*, 2016; Dinesh *et al.*, 2017; Tabone, Kiliccote, and Kara, 2018). Due to the focus on aggregated instead of individual PV power estimation, the approach proposed in this paper does not require access to smart meter data but instead works with aggregated measurements at the feeder head. PV power estimation can reduce the need for real time communication with metered installations, but is particularity useful for the case of installations which are not individually metered, i.e. behind-the-meter PV. A number of methods have been recently proposed in the literature for estimating the PV generation of a feeder, namely transposition model based approaches (Killinger *et al.*, 2016), data-driven based approaches (Shaker, Zareipour, and Wood, 2016b; Pierro *et al.*, 2017; Sossan *et al.*, 2018), and a hybrid of these approaches (Bright *et al.*, 2018).

Transposition model based approaches typically employ Global Horizontal Irradiance (GHI) measurements, map these measurements to both their Direct Normal Irradiance (DNI) and Direct Horizontal Irradiance (DHI) components, and then use a representative PV model to estimate power production.

[a)]Electronic mail: evrettos@lbl.gov; Corresponding author.
[b)]Electronic mail: eck@fastmail.com; This work was completed while E.C. Kara was still affiliated with SLAC National Accelerator Laboratory.
[c)]Electronic mail: stewart78@llnl.gov
[d)]Electronic mail: ciaran_r@berkeley.edu

The inaccuracy in estimating DNI and DHI from GHI measurements places an upper bound on the performance of these models (Lave *et al.*, 2015; Gueymard, 2010), which will be compounded for choice of model parameters (representative tilt, efficiency, etc.). For example, Ruf (2016) uses irradiance data based on satellite images together with reference PV models with known location and rated power, but with approximate azimuth and tilt angles, to estimate the power output of individual PV systems as well as the total PV power at the distribution substation. The analysis gave a normalized root mean squared error of 13% for the aggregate PV power, but also revealed systematic errors that result in overestimation of the total PV energy by approximately 22%.

Recently proposed methodologies to overcome the previously mentioned limitation have focused on data-driven approaches. In Shaker, Zareipour, and Wood (2016b), the authors adapt an up-scaling approach. They first determine geographic sub-regions of sufficient active power generation similarity using a hybrid of *k*-means clustering and Principal Component Analysis (PCA) proposed in Shaker, Zareipour, and Wood (2016a). Then, having learned the statistical properties of the aggregated generation for each sub-region from a sufficiently large subset of historical data, they use a small number of sites in each sub-region to estimate its respective total aggregate PV active power generation. The data used in Shaker, Zareipour, and Wood (2016b) were 15-minute active power generation data and subsequently exhibited temporal smoothing. The authors noted that new installations were incorporated by updating the effective capacity of its closest centroid cluster. The work in Pierro *et al.* (2017) clusters regions of similar power generation patterns and then adapts a neural network based approach to estimate either the PV active power generation of each cluster or the total power generation across all clusters. The authors found that using an individual neural network for each cluster achieved better performance. The data used were hourly PV generation profiles and therefore exhibited temporal smoothing. Additionally, the impact of new PV installations was not discussed. Sossan *et al.* (2018) considers higher frequency reporting and uses local GHI measurements to identify PV production patterns in aggregated net active power measurements of small geographic areas. Although the algorithms exhibited good performance for the cases considered, the authors noted that they expect performance to deteriorate as the geographic area increases due to the localized nature of GHI measurements.

In Bright *et al.* (2018) the authors adapt a hybrid approach blending satellite-derived GHI estimates and reference PV systems to estimate the PV generation of geographic areas. The authors spatially interpolate the difference between the measured PV output of the reference sites and the power predicted at those sites by satellite-derived GHI estimates. This gives a correction factor for each site of interest that itself is then spatially interpolated and applied to the satellite-derived PV generation of each site to give an estimate of a site's generation. The authors use satellite imagery from the state-of-the-art Himawari-8 satellite with a scan-rate of 10 minutes, which establishes the temporal resolution of the generation estimates. In contrast, in this work we are interested in an approach which leverages existing data sources readily available to system operators and minimizes additional data requirements, such as advanced satellite imagery. Additionally, we are interested in more granular PV generation profiles than currently attainable by satellite-derived GHI estimates in order to understand short-term variability and its impact on the operation of distribution voltage regulation equipment.

A related data-driven disaggregation approach is presented in Wang *et al.* (2018) that focuses on forecasting of net load. The authors decompose the net load measurements to actual load, PV output and a residual, forecast the individual components separately, and then add them to obtain the net load forecast. This process involves estimating the power capacity, tilt angle, and azimuth of a virtual equivalent PV system, which is modeled to approximate the total output of all PV installations. Wang *et al.* (2018) showcases how PV disaggregation methods can be useful not only for real-time estimation, but also for forecasting purposes.

Particularly relevant to our work is Kara *et al.* (2018), where the authors propose two methods to disaggregate PV power using aggregate active and reactive power measurements at a distribution substation. In addition, both methods require a rough estimate of irradiance called "irradiance proxy", which can be for example measurements of generated active power from a nearby monitored PV system. The first method of Kara *et al.* (2018) is a multiple linear regression estimator, which assumes that the prediction error of PV power is much larger than that of load power. The second method is a variant of the Contextually Supervised Source Separation (CSSS) methodology originally proposed in Wytock and Kolter (2014). CSSS is an optimization problem formulation that relies on regression models to disaggregate a single aggregate signal into a mixture of unobserved source signals. The advantage of CSSS is that it allocates the overall estimation error to each of the source signals systematically, by leveraging contextual information about them (such as smoothness). While Wytock and Kolter (2014) demonstrated CSSS for the energy disaggregation problem, Kara *et al.* (2018) modified CSSS for the PV disaggregation problem, where the aggregate signal is the aggregate active power measured at the feeder head and the source signals are the PV active power generation and load active power demand.

This paper builds on the results of Kara *et al.* (2018) and its contribution is multifold. First, we extend the optimization problem formulation of CSSS from Kara *et al.* (2018) by including regularization terms and time-varying regressors for PV and load power, as well as adding new regressors such as ambient temperature. Since CSSS is a multi-objective optimization problem, our second contribution is a parametric analysis to identify objective function weighting factors that maximize disaggregation accuracy without compromising robustness of results. Furthermore, if not retrained, the algorithm's performance degradation with respect to total installed PV power is lower than other data-driven approaches. This is a practical advantage and also applies to Sossan *et al.* (2018), which uses hyperparameters similar to our weighting factors. Moreover, we test the algorithm's performance in scenarios where the PV inverter provides reactive power support using

Volt-Var control. Finally, we investigate the performance of CSSS in estimating the total PV generation of a number of distributed PV systems, as opposed to Kara *et al.* (2018) that only considered a centralized large PV system. Our methodological improvements and detailed analyses on a much larger data set compared with Kara *et al.* (2018) allow us to thoroughly characterize the potential of CSSS as a real-time PV disaggregation method and benchmark it against a commonly-used transposition model-based approach.

The rest of this paper is organized as follows. In Section II we introduce the assumed system setup and available data for both the centralized and distributed PV system cases. Section III presents the regression models for PV and load power, as well as the optimization problem formulation for CSSS. Section IV discusses extensive simulation results and provides recommendations for real-world implementation, whereas Section V concludes.

II. SYSTEM SETUP AND DATA

A. Overview

Estimation of total PV power from substation-level aggregate power measurements improves situational awareness for utilities but is a challenging task. Besides spatial variability of solar irradiance due to cloud cover, the challenges are also related to non-linearities in PV power output of different systems at nearby locations due to differences in orientation and/or tilt angle, shading, and diverse inverter DC/AC ratios. In this paper, we consider two use cases: first, a single large PV system; and second, many small-scale PV systems connected downstream of a distribution substation. The second use case is more interesting from a practical point of view, however, the first case study is considered to enable an one-to-one comparison with the previous work Kara *et al.* (2018).

B. Single PV System Case

As a first case study, we consider a substation feeder from the territory of Riverside Public Utilities company (RPU) with the structure of Fig. 1. The feeder includes a PV system with 7.5 MWp capacity, South orientation, and a 7.5° tilt angle (see Table I). The PV system operates at a unity power factor, however, the effective power factor as seen from the grid side is variable because the PV system is connected to the grid through a transformer. In this setup, the PV system is the only generation asset connected to the substation. We have access to voltage and current phasor measurements at the feeder head from a Phasor Measurement Unit (PMU) located at the substation (denoted as PMU 1 in Fig. 1). Our goal is to disaggregate the PV power generation using the aggregate active and reactive power values computed from the PMU 1 measurements. Note that only data from PMU 1 are used as input to the real-time disaggregation method, whereas data from PMU 2 are only used for tuning optimization and performance evaluation purposes.

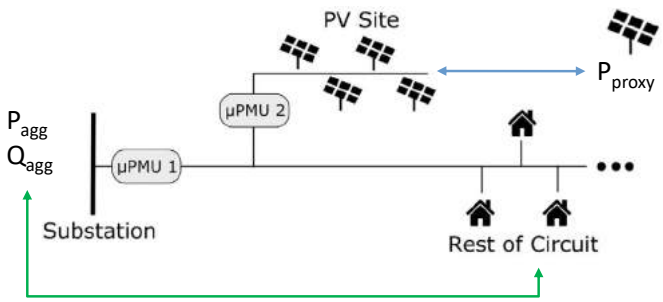

FIG. 1. System setup with a single PV system (utility-scale) showing the PMU locations. The proxy PV system is located nearby, but is not connected to the considered feeder. The blue arrow indicates that the power production of the unmonitored PV system is estimated based on active power measurements from the proxy PV system. The green arrow indicates that the total load power is estimated based on aggregate reactive power measurements from the PMU at the substation. More information on these modeling dependencies is given in Section III A.

TABLE I. Tilt and orientation (azimuth) information for PV systems.

	Orientation (°)	Tilt (°)	Distance (miles)
Main PV system	180 (South)	7.5	-
Irradiance proxy	195 (South-South-West)	20	4.5

Besides PMU measurements, an irradiance proxy is also needed for PV disaggregation. For example, measurements of active PV power generation from another monitored nearby PV system can be used as irradiance proxy. In our case study, the irradiance proxy measurements come from a PV system at the University of California Riverside's (UCR) Center for Environmental Research and Technology (CE-CERT) microgrid (Taylor *et al.*, 2016), which is located approximately 4.5 miles away from the RPU PV system and connected to a different feeder. The proxy PV system has a South-South-West orientation and a 20° tilt angle. Due to the small geographical distance between the two PV stations, the similar orientations[1], and the relatively small difference in tilt angles, this use case is relatively simple and thus the disaggregation results might not be generalizable for more complicated system setups. Nevertheless, this use case allows us to showcase the superior performance of the proposed method to that of Kara *et al.* (2018).

Unfortunately, no information on the DC/AC specifications and power ratings of the RPU and UCR PV systems is available, but such information is in fact not needed by the disaggregation method. However, without this information it is

[1] The available orientation information for the two PV systems is qualitative, i.e. we know that they both face generally towards the South, but the exact azimuth values were not available to us. With reference to Fig. 5 there is a shift in the solar peak, which indicates that in fact the azimuths are not exactly the same. The orientation angles reported in Table I were estimated using a data-driven approach in conjunction with visual inspection in Google Earth.

not possible to anticipate modified scaling factors between the unmonitored and proxy PV systems due to inverter clipping, especially in case of large DC/AC ratios. As a result, if inverter clipping occurs, PV disaggregation error is likely to increase. Nevertheless, this problem can be circumvented by using time-varying regressors, as proposed in this paper, which are expected to capture systematically modified PV scaling ratios due to inverter clipping.

The CSSS-based PV disaggregation method developed in this paper is validated on actual data measured by PMU 1 and PMU 2 for the whole months of August 2016 and January 2017. This paper presents a more in-depth analysis of CSSS performance in comparison with Kara *et al.* (2018), where a small data set with three days in June 2016 was used. Although the PMU data become available at a rate of 120 Hz, we down-sample them to a 1-minute resolution for disaggregation purposes. Note that the raw reactive power measurements from PMU 1 are distorted by capacitor bank switching events, which are filtered out from the reactive power time series using the algorithm presented in Kara *et al.* (2018).

One of our goals is to investigate whether it is possible to derive generic (or at least seasonal) parameterizations of the PV disaggregation algorithm, which result in low disaggregation error for a broad range of input data, namely PV and load profiles. For this reason, we generate ten training sets from the January and August data by randomly sampling ten subsets of fifteen days each from the full set of thirty-one days for each month. Most of the analysis of Section IV will be repeated for all ten training sets, as well as for the full data sets, in order to investigate how consistent the optimal weighting factors of the CSSS problem formulation are.

C. Distributed PV Systems Case

In practice, disaggregating PV power becomes more useful in systems with many unmonitored, residential-scale PV systems distributed along a feeder. To investigate CSSS performance in such cases, we additionally consider the system setup of Fig. 2, where we are interested in estimating the total generated power from all PV systems. The aggregate power measurements at the substation are the same as in the single PV system case of Section II B. However, we now assume that a small subset of all PV systems are monitored, and use their active power measurements as irradiance proxies to estimate the total PV power generation (which includes monitored and unmonitored PV systems).

As a case study, we use the total load power from the RPU substation feeder and 74 PV power profiles from the Pecan Street data set (available at dataport.cloud). The individual PV power profiles were scaled such that their total peak power across each month matches the respective peak power of the single 7.5 MWp PV system connected to the RPU feeder. Therefore, the new substation active power load demand is equal to the old load demand, minus the active PV power output of the RPU system, plus the scaled active power output of the distributed PV systems. Given that each installation was a residential installation, we assumed each system to operate

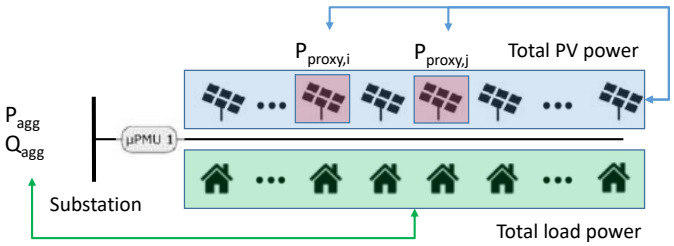

FIG. 2. System setup with many PV systems distributed along the feeder. A few PV systems are monitored (indicated with red-shaded boxes) and their power measurements are used to estimate the total PV power (shown with the blue-shaded box). This dependency is graphically shown with the blue arrows. The total load power (indicated with the green-shaded box) is estimated based on aggregate reactive power measurements from the PMU, and this dependency is shown with the green arrow. More information on these modeling dependencies is given in Section III A.

TABLE II. Percentage of distributed PV systems with each of the possible orientations.

Orientation	SW	S	W	WE	SE	E
Percentage	61.5%	21.7%	11.7%	1.7%	1.7%	1.7%

at unity power factor. Note that we did not consider the difference in power flow losses associated with having one large PV installation close to the substation v.s. a large number of smaller distributed installations. Using the same load power profile and scaling the generated PV power enables comparisons between the single PV system and distributed PV cases. The PV systems have various tilt angles (unknown) as well as various orientations with South-West being the most common (see Table II and note that exact azimuth information is not available). Due to these variations and the larger geographical dispersion, the results of this case study are more representative of real-world scenarios.

The 74 PV profiles were selected from a larger dataset by identifying PV systems which were likely from a similar geographic region using a clustering approach. A combination of dynamic time-warping (Keogh and Ratanamahatana, 2005) and $k-$means clustering was used to select a subset of the PV profiles to mimic the case of installations on the same distribution feeder. Figure 3 shows the PV active power profile for each of the 74 sites during a clear-sky day in August, where it can be seen that there is significant variation in orientation across the systems.

Previous studies show that high-frequency variations in PV generation are less spatially correlated than lower-frequency variations (Mills and Wiser, 2010). This is mostly due to cloud movements that can create very localized sudden drops in PV power production. Therefore, using the raw irradiance proxy measurements might introduce error in estimating the power of the unmonitored PV systems. To remove the effect of high-frequency variations in PV power generation, we smooth out the individual irradiance proxy active power measurements using a five-minute average filter. Note that if the averaging period is set too high, then useful information in

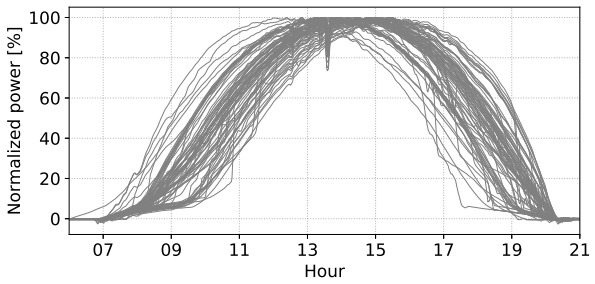

FIG. 3. Normalized power of all 74 PV systems for one clear-sky day in August. The PV power is normalized by the maximum PV generation of each site on that particular day.

the irradiance proxy measurements that would otherwise help inform the PV disaggregation will be lost. We selected an averaging period of five minutes because this was also the case in the previous work Kara *et al.* (2018). Investigating the effect of the averaging period on algorithm performance is left for future work.

D. Assumptions on Availability of Measurements

In Section III, five variants of the proposed PV disaggregation method will be presented. All variants assume access to *real-time* aggregate active and reactive power measurements at the feeder head, as well as irradiance proxy measurements (active power of one or more PV systems). Real-time here is relative to the desired resolution of the disaggregated PV profile. For example, to disaggregate PV power with 1 minute resolution, the measurements should be received every 1 minute or faster. Two of the method variants additionally assume access to ambient temperature measurements, which of course can be updated at a lower frequency (e.g., every 15 minutes or 1 hour). Theoretically, the proposed method can work with only the above mentioned measurements, i.e. even if a large portion of the PV systems are not monitored at all.

However, as it will be shown in Sections III and IV, PV disaggregation is formulated as a multi-objective optimization problem and good performance is conditional on appropriate tuning of the objective function's weighing factors. For weight tuning purposes, access to separate ground truth data of aggregate PV active power and aggregate load active power at the feeder head is essential. This requires active power data to be collected locally at each PV station and sent periodically to the central location hosting the PV disaggregation method. Nevertheless, weight tuning and thus access to locally monitored PV data is required very infrequently (e.g. on an annual basis), which drastically reduces communication burden, as discussed in Section IV I 2.

III. PV DISAGGREGATION METHOD

A. Basic Modeling

We use a linear model to capture the dependence between the PV power $P_{\mathrm{PV},t}$ and the irradiance proxy ϕ_t (i.e. the active power measurements from the nearby monitored PV system)

$$P_{\mathrm{PV},t} = C_{\mathrm{PV},t}\ \phi_t + \varepsilon_{\mathrm{PV},t}\ , \tag{1}$$

where $C_{\mathrm{PV},t}$ is the coefficient on the irradiance proxy, and $\varepsilon_{\mathrm{PV},t}$ is the error in PV predictions. Note that the regressor $C_{\mathrm{PV},t}$ can be time-varying in general in order to capture any dominant intra-day patterns. In principle, time-varying regressors can help us work around systematic errors that occur in case of inverter clipping or if the orientation, tilt, or shading conditions of the irradiance proxy are significantly different to the ones of the non-monitored PV system. For example, using time-varying regressors allows us to correct for the fact that the peak power of a non-monitored PV system with west orientation will come later in the day compared with a nearby PV system with east orientation.

The load active power consumption $P_{\mathrm{L},t}$ is modeled in a similar way using

$$P_{\mathrm{L},t} = C_{\mathrm{L},t}\ Q_{\mathrm{PMU}_1,t} + R_{\mathrm{L},t} + \varepsilon_{\mathrm{L},t}\ , \tag{2}$$

where $C_{\mathrm{L},t}$ is the coefficient on the aggregate reactive power measured by PMU 1 ($Q_{\mathrm{PMU}_1,t}$), $R_{\mathrm{L},t}$ is an intercept term that

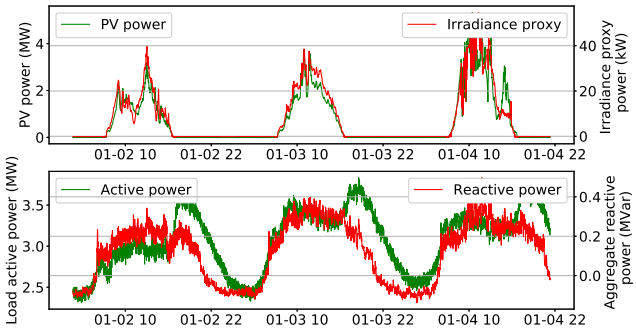

FIG. 4. Time series of dependent and independent variables of the regression in January. Top: PV power vs irradiance proxy. Bottom: Load active power vs aggregate reactive power.

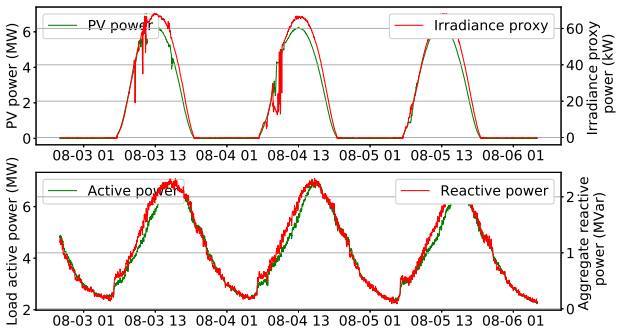

FIG. 5. Time series of dependent and independent variables of the regression in August. Top: PV power vs irradiance proxy. Bottom: Load active power vs aggregate reactive power.

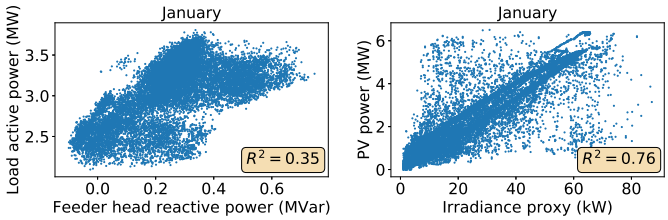

FIG. 6. Testing of linear dependence hypothesis in January. Left: Load power vs aggregate reactive power. Right: PV power vs irradiance proxy.

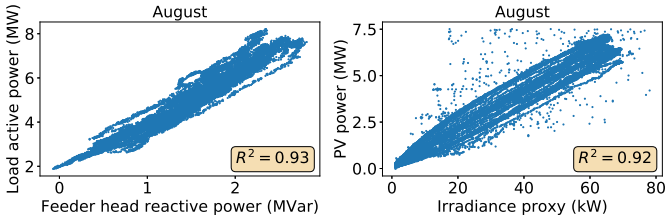

FIG. 7. Testing of linear dependence hypothesis in August. Left: Load power vs aggregate reactive power. Right: PV power vs irradiance proxy.

represents purely resistive load in the system, and $\varepsilon_{\mathrm{L},t}$ is the error in load predictions. The aggregate reactive power is a good proxy for the load active power as it captures its dependence on the power factor. Note that $P_{\mathrm{L},t}$ is assumed to be positive and $P_{\mathrm{PV},t}$ negative in the rest of the paper.

To justify the used linear regression models, Figs. 4 and 5 plot the PV and load power (from the single PV system case study) together with their respective regressors, whereas Figs. 6 and 7 present the same data in the form of scatter plots. It can be seen that the linear correlation between the PV power and irradiance proxy is strong in August, and weaker in January (but still significant). Of course, there exist differences in the patterns of PV power and irradiance proxy in both months due to passing clouds and different orientations and tilt angles. The dependence between the load power and reactive power at the feeder head is notably linear in August, but rather weak in January when the reactive power time series is noisy, as shown in Fig. 4. These differences are expected to require separate parameterization and tuning of the disaggregation problem for each of the considered months.

B. Temperature as Additional Regressor

Model (2) assumes access to exactly the same data sources as in Kara *et al.* (2018), namely Phasor Measurement Unit (PMU) measurements. In this section, we add ambient temperature $T_{\mathrm{a},t}$ as an additional regressor, which leads to the following updated linear load model

$$P_{\mathrm{L},t} = C_{\mathrm{L},t}\, Q_{\mathrm{PMU}_1,t} + \tilde{C}_{\mathrm{L},t}\, T_{\mathrm{a},t} + R_{\mathrm{L},t} + \varepsilon_{\mathrm{L},t}\ , \qquad (3)$$

where $\tilde{C}_{\mathrm{L},t}$ is the ambient temperature linear coefficient. Note that ambient temperature was also considered in the recent

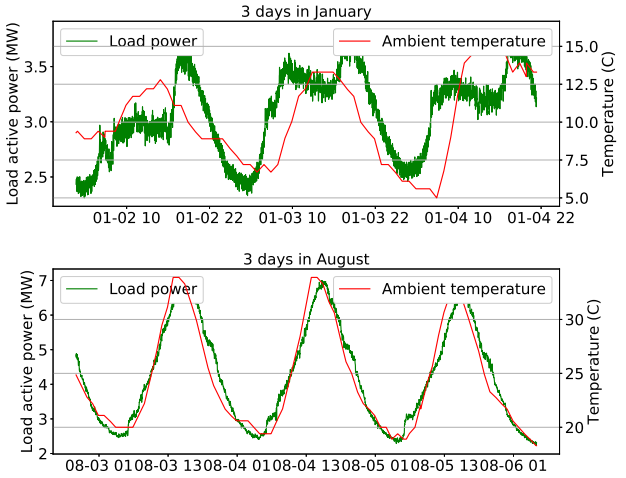

FIG. 8. Load active power versus ambient temperature in January (top) and August (bottom).

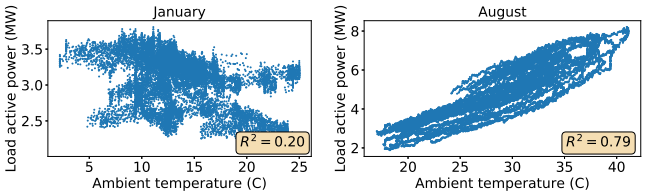

FIG. 9. Testing of linear dependence hypothesis between load active power and ambient temperature. Left: January. Right: August.

work Tabone, Kiliccote, and Kara (2018), which focused on the problem of estimating the production of individual behind-the-meter PV systems using substation measurements and data from Advanced Metering Infrastructure (AMI). In contrast, this paper focuses on estimation of aggregated PV power at the substation level and thus AMI information is not required.

In Fig. 8 we plot the load power against ambient temperature data from a nearby weather station (we show only 3 days for each month). The full monthly data are shown in the scatter plots of Fig. 9. Note that the raw ambient temperature data have a resolution of 1 hour, and are up-sampled to 1 minute using linear interpolation. Observe that the correlation between ambient temperature and load power is positive and strong in August, likely due to increased operation of air conditioning loads. The correlation is negative and weaker in January, possibly due to operation of space heaters.

Even though the ambient temperature does not affect the short-term variations in PV power, it can in principle improve disaggregation performance by capturing any temperature-dependent loads. In Section IV E 2, we will investigate in simulation the benefit of adding ambient temperature as an additional regressor in the load model only.

C. Contextually Supervised Source Separation (CSSS)

PV and load disaggregation can be achieved by first combining the models (1) and (2) to predict the aggregate active power measured by PMU 1

$$P_{\mathrm{PMU}_1,t} = P_{\mathrm{L},t} + P_{\mathrm{PV},t} \tag{4}$$

using ordinary least squares, and then reconstructing the PV and load profiles by assuming $\varepsilon_{\mathrm{L},t} \ll \varepsilon_{\mathrm{PV},t}$, as done in Kara *et al.* (2018). The authors of Kara *et al.* (2018) present also another approach to reconstruct the PV and load profiles, which distributes $\varepsilon_{\mathrm{L},t}$ and $\varepsilon_{\mathrm{PV},t}$ systematically, and is based on the CSSS methodology originally proposed in Wytock and Kolter (2014). In the following, we modify the general formulation from Kara *et al.* (2018); Wytock and Kolter (2014) for the PV disaggregation problem at hand.

CSSS disaggregates the measured $P_{\mathrm{PMU}_1,t}$ to the unknown signals (or sources) $P_{\mathrm{L},t}$ and $P_{\mathrm{PV},t}$ by solving the optimization problem

$$\begin{aligned}
\min_{x}\ & \alpha_{\mathrm{PV}} \cdot \ell(\varepsilon_{\mathrm{PV},t}) + \alpha_{\mathrm{L}} \cdot \ell(\varepsilon_{\mathrm{L},t}) + && \text{(5a)}\\
& \beta_{\mathrm{PV}} \cdot h(C_{\mathrm{PV},t}) + \beta_{\mathrm{L}} \cdot h(C_{\mathrm{L},t}, \tilde{C}_{\mathrm{L},t}, R_{\mathrm{L},t}) + && \text{(5b)}\\
& \gamma_{\mathrm{PV}} \cdot g(P_{\mathrm{PV},t}) + \gamma_{\mathrm{L}} \cdot g(P_{\mathrm{L},t}) && \text{(5c)}\\
\text{s.t. } & P_{\mathrm{PMU}_1,t} = P_{\mathrm{L},t} + P_{\mathrm{PV},t},\ \forall t && \text{(5d)}\\
& P_{\mathrm{PV},t} \le 0,\ \forall t && \text{(5e)}\\
& P_{\mathrm{L},t} \ge 0,\ \forall t\ , && \text{(5f)}
\end{aligned}$$

where $x = \{P_{\mathrm{PV},t}, P_{\mathrm{L},t}, C_{\mathrm{PV},t}, C_{\mathrm{L},t}, \tilde{C}_{\mathrm{L},t}, R_{\mathrm{L},t}\}$. The objective function consists of three terms. The function ℓ in (5a) is called loss function and penalizes the error between the reconstructed signals and the linear models (1) and (2). The weighting factors α_{PV} and α_{L} are design parameters and determine how much the modeling errors influence the objective function. Specifically, a relatively higher α_{PV} weight forces the optimizer to trust the PV model more than the load model, and vice versa. In contrast to Kara *et al.* (2018) that considered only the ℓ_2 norm, in this paper we consider both ℓ_1 and ℓ_2 norms as loss functions. The function g in (5b) is a regularization term that captures additional contextual information on source signals, such as smoothness. The function h in (5c) is another regularization term on the linear model parameters to avoid overfitting, which is important in case time-varying regressors are used. Expressions for the functions g and h will be given in Sections IV C and IV D. The weighting factors β_{PV}, β_{L}, γ_{PV} and γ_{L} are design parameters and reflect the level of confidence on the contextual information on PV and load profiles. Although included in the mathematical formulation, the regularization functions g and h were not considered in the numerical simulations presented in Kara *et al.* (2018).

Constraint (5d) ensures that the disaggregated signals recover the measured aggregate signal. Constraint (5e) requires that the PV signal is negative, whereas (5f) requires that the load signal is positive, which is the convention used in this paper. Note that constraints (5e) and (5f) were not included in the formulation of Kara *et al.* (2018). In Section IV, we will investigate the effect of adding these constraints on disaggregation performance. Optimization problem (5) is implemented in Python and solved using the MOSEK solver through a CVXPY interface (Diamond and Boyd, 2016). Note that only daytime is included in the optimization problem. Results on computational cost are reported in Section IV F.

D. CSSS for the Distributed PV Case with Multiple Irradiance Proxies

As mentioned in Section II C, more than one irradiance proxies might be used in case of distributed PV systems with various orientations. In this case, the PV model will look like

$$P_{\mathrm{PV},t} = C_{\mathrm{PV},t}^{(1)}\ \phi_t^{(1)} + \ldots + C_{\mathrm{PV},t}^{(N_\mathrm{p})}\ \phi_t^{(N_\mathrm{p})} + \varepsilon_{\mathrm{PV},t}\ , \tag{6}$$

where $\phi_t^{(i)}$ is the i$^{\text{th}}$ proxy and $C_{\mathrm{PV},t}^{(i)}$ is its regressor. Equation (6) implies that only one source signal is used for the total PV power production. An alternative approach would be to consider separate PV source signals for each of the orientations modeled by the N_p individual proxies. In that case, N_p different PV models would be needed

$$P_{\mathrm{PV},t}^{(i)} = C_{\mathrm{PV},t}^{(i)}\ \phi_t^{(i)} + \varepsilon_{\mathrm{PV},t}^{(i)}\ , \tag{7}$$

with $i \in [1, N_\mathrm{p}]$. The advantage of (7) is that it distributes the prediction errors $\varepsilon_{\mathrm{PV},t}^{(i)}$ separately for each orientation. The disadvantage is an increased number of terms in the objective function of (5) and the associated increased weight tuning burden. One possible solution is to determine the weighting factors proportionally to the percentage of PVs with each orientation, however, orientation information might not be available for all PVs. Due to these complexities, the simpler approach of (6) was used in this paper.

IV. RESULTS

A. Error Metrics

The performance of PV disaggregation is evaluated using the Root Mean Squared Error (RMSE) as a metric, which is defined as

$$\mathrm{RMSE} = \sqrt{\frac{\sum_{t=1}^{T}(\hat{P}_{\mathrm{PV},t} - P_{\mathrm{PV},t})^2}{T}}, \tag{8}$$

where $P_{\mathrm{PV},t}$ is the actual PV power, $\hat{P}_{\mathrm{PV},t}$ is the estimated PV power, and T is the number of data points. In addition, we use two different definitions of the normalized Root Mean Squared Error (nRMSE). In the first definition, the absolute RMSE value is normalized by the average value of load power in the considered period of time, $\bar{P}_\mathrm{L}$, as follows

$$\mathrm{nRMSE}_1 = \frac{\mathrm{RMSE}}{\bar{P}_\mathrm{L}}. \tag{9}$$

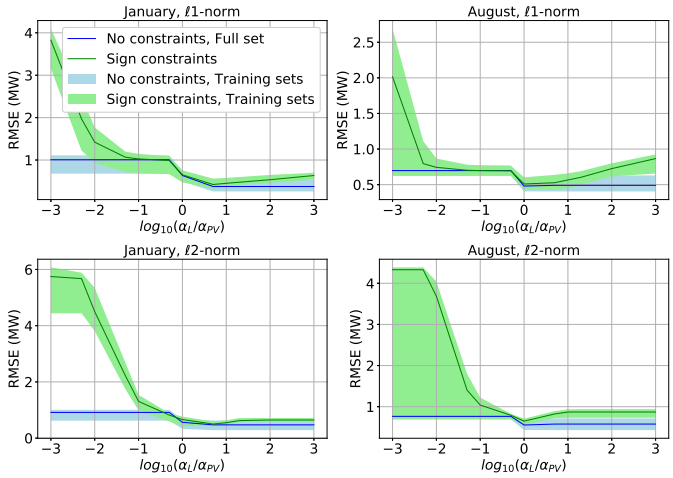

FIG. 10. Dependence of disaggregation RMSE on the α_L/α_{PV} ratio, with and without sign constraints. The top plots show results using ℓ_1 norm as loss function, whereas the bottom plots use ℓ_2 norm. The left plots are for January, whereas the right ones are for August.

In the second definition, the total installed PV power, $P_{PV,inst}$, is used for the normalization as follows

$$\text{nRMSE}_2 = \frac{\text{RMSE}}{P_{PV,inst}}. \tag{10}$$

B. Choice of Loss Function

In this section, we investigate the dependence of disaggregation performance on the choice of loss function (ℓ_1 or ℓ_2 norm) and the weighting factor values, as well as on whether the sign constraints (5e) and (5f) are included or not. The analysis is performed separately for each month, which results in four sets of simulations: (i) ℓ_1 norm in January, (ii) ℓ_2 norm in January, (iii) ℓ_1 norm in August, and (iv) ℓ_2 norm in August. For each of these cases, simulations are performed with and without sign constraints, whereas the α_L/α_{PV} ratio is varied in the range $[10^{-3}, 10^{3}]$ (with $\min[\alpha_L, \alpha_{PV}] = 1$). For the simulations of this section, the regularization terms (5b) and (5c) are omitted.

The simulation results are presented in Fig. 10, where the prediction RMSE is plotted as a function of the α_L/α_{PV} ratio.[2] The solid lines correspond to the full set of thirty-one days for each of the two months. The shaded areas show the RMSE range covered by each of the considered ten training sets, as described in Section II B. The best α_L/α_{PV} ratios and corresponding minimum RMSEs for each case are summarized in Table III.

A first observation is that larger α_L/α_{PV} ratios tend to decrease the prediction errors, which means that the linear regression model for the load should be generally trusted more than that for the PV. The best α_L/α_{PV} ratio depends on the month: it is 5 in January and 1 in August. Using a higher α_L/α_{PV} ratio in January can be justified by the fact that the linear dependence between the PV power and irradiance proxy is weaker, as shown in Fig. 6, given increased short-term cloud cover. A second observation is that using ℓ_1 norm as loss function gives consistently better results compared with ℓ_2 norm. Specifically, using the average load power for each month (3,056 kW in January and 4,931 kW in August) for normalization, the normalized RMSE (nRMSE) decreases from 15.4% in January and 11.3% in August with ℓ_2 norm to 12.3% in January and 9.7% in August with ℓ_1 norm. Table III additionally presents the normalized RMSEs obtained using the installed PV power for normalization (7.5 MW). Note that the nRMSEs in August are smaller than those in January due to the stronger linear correlations in August, as shown in Section II. Last, we find that omitting the sign constraints (5e) and (5f) gives better results, which is counterintuitive.

TABLE III. The best α_L/α_{PV} ratios and corresponding RMSEs (in kW, in % of average load $\bar{P}_L$, and in % of installed PV power $P_{PV,inst}$) with ℓ_1 and ℓ_2 norm for loss function in January and August.

		January		August	
ℓ_1 norm	sign constraints	no	yes	no	yes
	RMSE (kW)	376	423	480	508
	nRMSE_1 (% of $\bar{P}_L$)	12.3	13.8	9.7	10.3
	nRMSE_2 (% of $P_{PV,inst}$)	5.0	5.6	6.4	6.8
	α_L/α_{PV}	5	5	1	1
ℓ_2 norm	sign constraints	no	yes	no	yes
	RMSE (kW)	472	500	555	650
	nRMSE_1 (% of $\bar{P}_L$)	15.4	16.4	11.3	13.2
	nRMSE_2 (% of $P_{PV,inst}$)	6.3	6.7	7.4	8.7
	α_L/α_{PV}	5	5	1	1

Using an ℓ_2 norm without sign constraints is exactly the same disaggregation method as the one implemented in Kara *et al.* (2018), which reported an nRMSE of 6% (normalized by the installed PV power). The nRMSEs computed here are slightly higher (6.3% kW in January and 7.4% kW in August). This discrepancy is due to the different data sets used in the two works, as well as the fact that the PV data for the irradiance proxy were filtered using a 5-minute filter before being used in CSSS in Kara *et al.* (2018), but not in this paper.

C. Source Regularization

The goal of this section is to investigate to what extent adding the source regularization terms (5c) improves performance. Source regularization penalizes the difference between two consecutive values of the source signal[3], and we

[2] Timeseries results for the disaggregated PV and load signals will be shown in Section IV F together with the other CSSS variants presented later in the paper.

[3] Recall that the CSSS optimization problem is formulated and solved considering only daytime. Therefore, the source signal time series include discontinuities from evening of day d to morning of day $d+1$. Special care has been taken to avoid penalizing these discontinuities in (11).

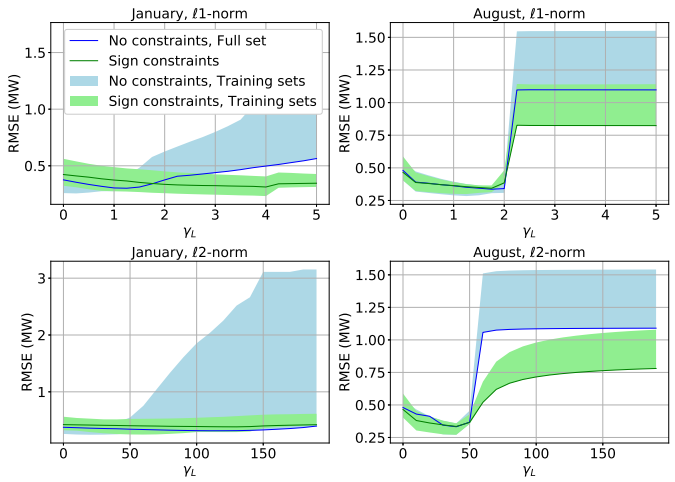

FIG. 11. The dependence of RMSE on load regularization factor γ_L, with and without sign constraints. The top plots show results using ℓ_1 norm, whereas the bottom plots use ℓ_2 norm. The left plots are for January, whereas the right ones are for August.

consider both ℓ_1 norm and ℓ_2 norm as penalty functions, i.e.

$$g(P_{L,t}) = \text{diff}(P_{S,t})_* \,, \tag{11}$$

where diff is the vector difference operator, $P_{S,t}$ is either $P_{L,t}$ or $P_{PV,t}$, and $*$ is either 1 or 2. Based on the results of Section IV B, we use ℓ_1 norm as loss function and fix α_L/α_{PV} to 5 in January and 1 in August. Similarly to Section IV B, the simulations are performed with and without sign constraints.

Preliminary simulations showed that source regularization helps if applied only to the load demand but not the PV generation. This can be explained by the fact that (except for cloud-free days) the load demand profile is generally smoother in comparison with the PV power profile. Therefore, we set $\gamma_{PV} = 0$, vary γ_L in the range $[0,5]$ for ℓ_1 norm and in the range $[0,175]$ for ℓ_2 norm (these ranges were identified with trial and error), and present the results in Fig. 11. The best γ_L and corresponding RMSEs for each case are summarized in Table IV.

TABLE IV. The best γ_L weighting factors for load power regularization and the corresponding minimum RMSE (in kW, in % of average load $\bar{P}_L$, and in % of installed PV power $P_{PV,inst}$) values with ℓ_1 norm and ℓ_2 norm for source regularization in January and August.

		January		August	
	sign constraints	no	yes	no	yes
ℓ_1 norm	RMSE (kW)	302	317	336	344
	nRMSE$_1$ (% of $\bar{P}_L$)	9.9	10.4	6.8	7.0
	nRMSE$_2$ (% of $P_{PV,inst}$)	4.0	4.2	4.5	4.6
	γ_L	1.25	4	1.75	1.75
	sign constraints	no	yes	no	yes
ℓ_2 norm	RMSE (kW)	315	384	332	335
	nRMSE$_1$ (% of $\bar{P}_L$)	10.3	12.6	6.7	6.8
	nRMSE$_2$ (% of $P_{PV,inst}$)	4.2	5.1	4.4	4.5
	γ_L	110	130	40	40

Observe that the ℓ_1 norm for load regularization achieves better results in January, whereas the ℓ_2 norm performs better in August. Nevertheless, the ℓ_1 norm has smaller variance in the γ_L values that achieve optimal performance in comparison with the ℓ_2 norm, as shown in Table IV. Furthermore, omitting the sign constraints gives better results (especially in January), but the differences are small if the ℓ_1 norm is used. However, note that adding the sign constraints increases robustness to non-optimal selection of the γ_L value: with reference to Fig. 11, the worst-case RMSEs with sign constraints are smaller as γ_L approaches 5. Based on these findings, we suggest using ℓ_1 norm for load regularization, and including the sign constraints to reduce the risk of getting bad results.

D. Time-Varying Regressors and Regressor Regularization

In this section, we investigate the effect of using time-varying regressors in the linear models (1) and (2), which were assumed to be time-invariant in the analysis so far. For this purpose, we split the day into a number of time windows and allow the optimization to determine different regressor values for each window. Clearly, this gives an additional degree of freedom when fitting the models, but at the same time increases the risk of overfitting.[4] Therefore, we penalize the regressor changes from one window to the next one by using the following regularization terms

$$h(C_{PV,t}) = \text{diff}(C_{PV,t})_1 \tag{12a}$$
$$h(C_{L,t}, R_{L,t}) = \text{diff}(C_{L,t})_1 + \text{diff}(R_{L,t})_1 \,. \tag{12b}$$

We investigate the following cases of using time-varying regressors: (i) only for the PV model, (ii) only for the load model, and (iii) for both models. For each case, we run simulations with different number of windows while varying the weighting factors β_{PV} and/or β_L in the range $[0, 10^6]$. Note that the ranges of β_{PV} and β_L are several orders of magnitude larger than those of α_L, $/\alpha_{PV}$ and γ_L, because they penalize regressors with numerical ranges smaller than those of the source signals (load and PV profiles). To keep the total number of simulations reasonable, only the full data sets in January and August are used in this investigation, i.e. the training sets are not considered. The ℓ_1 norm is used as loss function with α_L/α_{PV} fixed according to Table III, and source regularization for load demand is also used as in Section IV C.

Fig. 12 presents the results for January and August with regressor regularization applied only to the PV power profile. In January, the lowest errors are obtained when using 2 windows and weighting factors in the range $0 - 10^4$. In August, 2 windows and a weighting factor of 10^4 are the best options, whereas increasing the number of windows reduces performance significantly. Overall, the contribution of time-varying

[4] In addition, non-negativity and non-positivity constraints were imposed to the load power and PV power regressors, respectively. Adding these constraints in (5) did not have a major effect in the results; however, it was shown to avoid unrealistic solutions if smaller data sets are used.

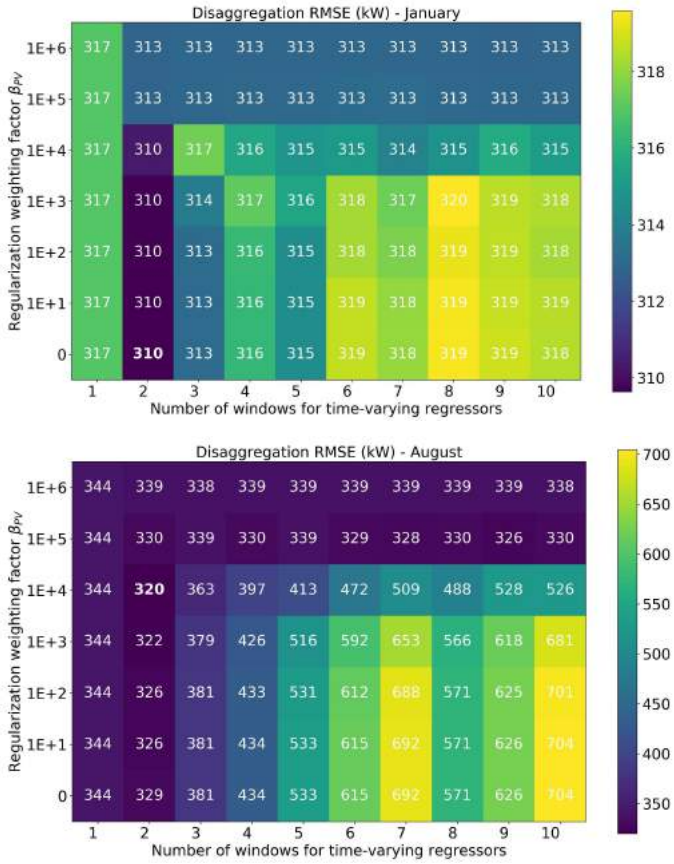

FIG. 12. Disaggregation performance for different combinations of time windows and regularization factors for solar power in January (top) and August (bottom).

regressors is relatively small in this case study: in January, RMSE reduces from 317 kW to 310 kW (2% improvement), whereas in August, it reduces from 344 kW to 320 kW (7% improvement).

Although some general patterns are visible in Fig. 12, RMSE does not vary smoothly with β_{PV} and the number of windows, but instead local minima can be observed. For example, six windows perform worse than five but better than seven in August. Such local minima are more pronounced with smaller β_{PV} values and suggest overfitting issues. For a given number of windows, when we increase β_{PV} towards the boundary value of 10^6 we approach the one-window solution, which is to be expected due to the large penalty on regressor value changes. Finally, using time-varying regressors for load power only or for both PV and load power gives worse results, which are omitted for brevity.

E. Additional Regressors

1. Overview

In this section, we investigate the performance of three variants of the CSSS optimization problem (5). The first variant uses the extended load model with dependence on ambient temperature, the second variant allows the optimal solution to comprise different regressors for weekdays and weekends, and the third variant is a combination of the first and second variants.

TABLE V. Disaggregation RMSE for the basic model, the model with ambient temperature (Ta) as a regressor, the model with separate regressors for weekdays and weekends (Day-of-Week - DoW - index), and the model with both Ta and DoW. The cases A, B and C are defined in Section IV E.

Case	January (RMSE in kW)				August (RMSE in kW)			
	Basic model	Ta	DoW	Both	base case	Ta	DoW	Both
A	423	364	206	189	508	528	529	517
B	317	263	202	205	344	343	369	379
C	310	243	201	199	320	334	331	358

The three CSSS variants are compared with the original CSSS formulation that uses the basic model (2). The comparison is performed for the following cases of the CSSS optimization problem formulation:

(A): Loss function only

(B): A + Source regularization for load power

(C): B + Time-varying regressors + Regressor regularization for PV power.

The weighting factors for loss function and regularization terms, as well as the number of windows for time-varying regressors, are fixed to the optimal values identified with the previous analyses.

2. Ambient Temperature

Table V compares the solar disaggregation results of the basic load model (2) with those of the load model (3) with ambient temperature as an additional regressor. In January, using ambient temperature reduces the RMSE in all cases (error reduction in the range $14-23\%$), however, RMSE increases slightly in August. With reference to Figs. 8 and 9, this result might seem counterintuitive at the first glance, because the linear dependence between load power and ambient temperature is much stronger in August than in January. Nevertheless, this result can be explained by comparing the R^2 values shown in Figs. 6, 7 and 9. In August, the correlation of load power with reactive power measured at feeder head is very high ($R^2 = 0.93$) and higher than the correlation with ambient temperature ($R^2 = 0.79$), and both correlations are positive. In January, the correlation of load with reactive power is rather low ($R^2 = 0.35$), and even though the correlation with ambient temperature is lower ($R^2 = 0.2$), the overall performance improves because the correlation directions of the two independent variables are opposite.

3. Separate Regressors for Weekdays and Weekends

Since there is typically a weekday-weekend pattern in load demand, we investigate using different optimization variables

TABLE VI. Parameters of the different linear models used in January (linear coefficients for aggregate reactive power and ambient temperature, and intercept terms), RMSE and solution time.

Case	Load model			PV model		RMSE	Improve-	Time
	C_{L}	$\tilde{C}_{\mathrm{L}}$	R_{L}	$C_{\mathrm{PV},t}$		(kW)	ment (%)	(s)
A	2.04	–	2812.64	-100.96		423	N/A	2.6
B	0.80	–	2945.60	-93.19		317	25.1	1.4
C	0.85	–	2927.79	-96.17	-89.36	310	26.7	1.4
D	0.94	-26.54	3212.23	-94.62	-85.78	243	42.6	1.6
E	$1.24 \cdot 10^{-6}$ $-1.68 \cdot 10^{-6}$	-10.88 3.15	3400.90 2366.95	-90.60	-85.90	199	53.0	1.7

TABLE VII. Parameters of the different linear models used in August (linear coefficients for aggregate reactive power and ambient temperature, and intercept terms), RMSE and solution time.

Case	Load model			PV model		RMSE	Improve-	Time
	C_{L}	$\tilde{C}_{\mathrm{L}}$	R_{L}	$C_{\mathrm{PV},t}$		(kW)	ment (%)	(s)
A	2.55	–	1524.34	-107.08		508	N/A	2.5
B	2.48	–	1487.38	-104.28		344	32.3	1.9
C	2.31	–	1659.11	-107.08	-96.41	320	37.0	2.0
D	2.36	-7.51	1782.19	-106.91	-96.02	334	34.3	2.1
E	2.75 2.42	-49.03 21.19	2330.37 1110.97	-106.39	-97.06	358	29.5	2.1

for the regressors of weekdays and weekends. We simulate cases A, B and C as described in Section IV E and report the results in Table V. In August, the results are slightly worse compared with the basic model, but in January they are significantly better (also better than those obtained when using ambient temperature as regressor). The reason is that the relative difference between average load power in weekdays and weekends is larger in January (see Figs. 13 and 14). Finally, Table V also shows simulation results with both modifications of this section applied (ambient temperature and weekday-weekend dependence). Note that combining the two modifications does not improve performance in August. However, there is a further improvement in the results in January.

F. Disaggregation and Computational Cost Results of Selected Models

We present the fitted linear model parameters and time-domain disaggregation results for cases A - C of Section IV E, as well as for the following cases:

(D): C + Ambient temperature as additional regressor

(E): D + Separate regressors for weekdays and weekends.

The model parameters are given in Tables VI and VII for January and August, respectively. The two values for $C_{\mathrm{PV},t}$ for cases C, D and E correspond to the two time windows used. The first row of case E shows the load model parameters for weekdays, whereas the second row corresponds to weekends. The RMSE values are repeated for convenience and the relative improvements with respect to Case A (simplest formulation with loss function only) are computed.

The time needed to solve the CSSS disaggregation problem for the full month is also shown in Tables VI and VII. The optimization problem is solved using a laptop with 6 cores, 2.6 GHz processor base frequency, and 16 GB RAM. The fast solution times allow the method to be used for nearly real-time PV disaggregation purposes. It is interesting to note that, besides improving disaggregation performance, the enhancements of cases B - E also reduce solution time with respect to the base formulation of case A, despite the fact that the objective function is more complex and/or the decision vector is larger. This is due to the enhancements of cases B - E that make the objective function “steeper" and increase convergence rate to the optimal solution.

The load and PV measured data as well as the estimated time series with CSSS for all five cases are plotted in Figs. 13 and 14 for January and August, respectively. We can see that Case A results in the largest discrepancies between the estimated and actual load and PV power. In January, the best results are achieved in Case E, mainly by improving load disaggregation on Saturday and Sunday. However, the applied weighing factor for source regularization ($\gamma_{\mathrm{L}} = 4$) might be too high for Case E, as indicated by the flat lines in estimated load power at daytime (especially on the weekend). Note that the jumps in estimated power that often appear around 08:00 and 17:00 are due to the fact that CSSS disaggregation is applied for daytime only. In August, the PV and load profiles are generally smoother. Note that disaggregation errors increase in Case A at intervals with spikes in PV power output, e.g., around 09:00 - 10:00 on Thursday, August 4. On the other hand, Cases B - E produce smoother results and reduce disaggregation error.

In summary, the proposed method’s RMSE is 3.5% on average (2.6% in January and 4.3% in August), which is lower

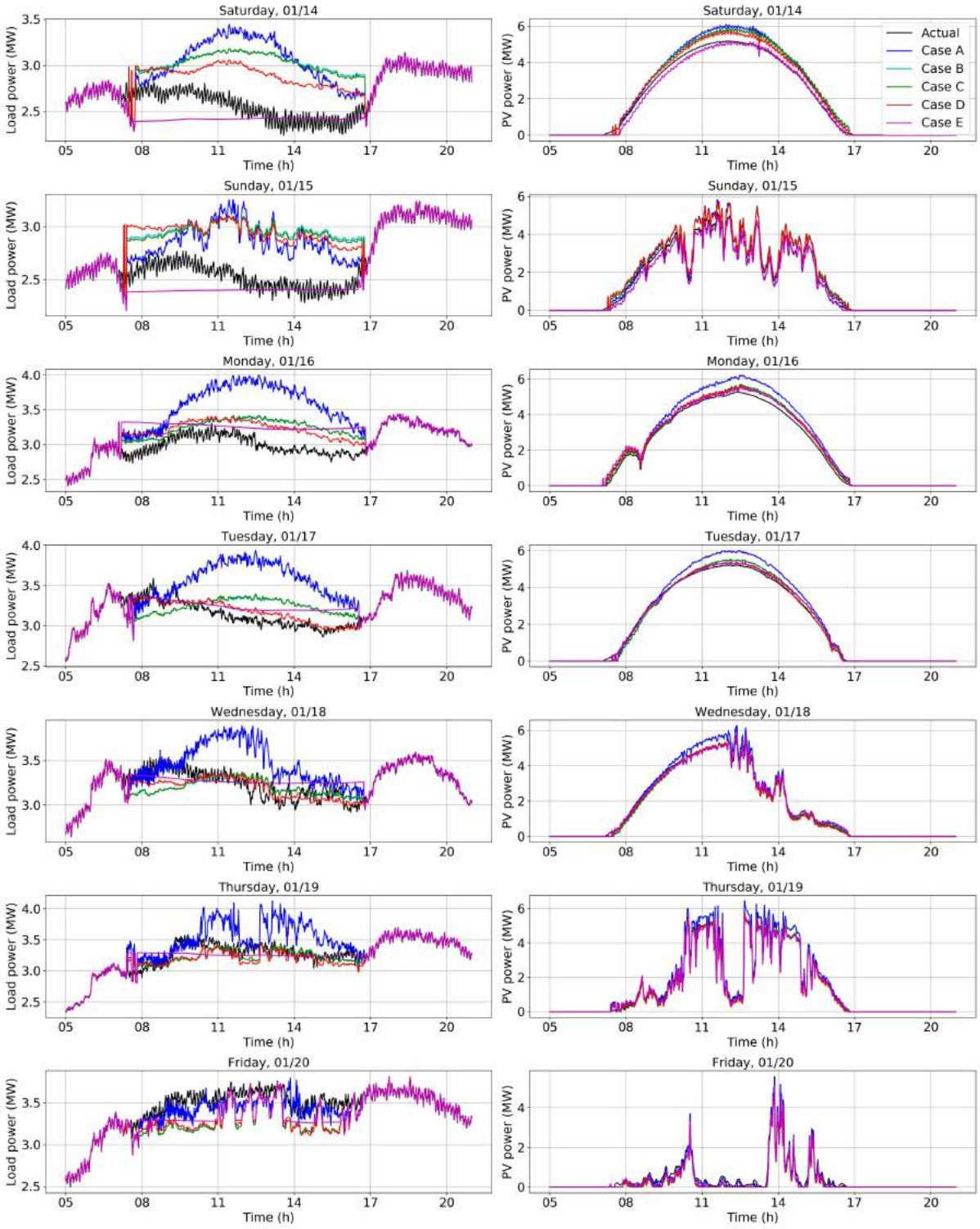

FIG. 13. Actual and disaggregated load power (left plots) and PV power (right plots) for one week in January. Disaggregation results are shown for cases A - E of Table VI.

compared with the earlier work Kara *et al.* (2018) that reported an RMSE of 6% on a three-day dataset. The previously mentioned RMSE values are normalized by the installed PV power, which is 7.5 MW in both cases. Nevertheless, when applying the method of Kara *et al.* (2018) on the dataset used in this paper, the resulting RMSE was found to be 6.9% on average (6.3% in January and 7.4% in August). Therefore, the proposed method was shown to improve disaggregation per-

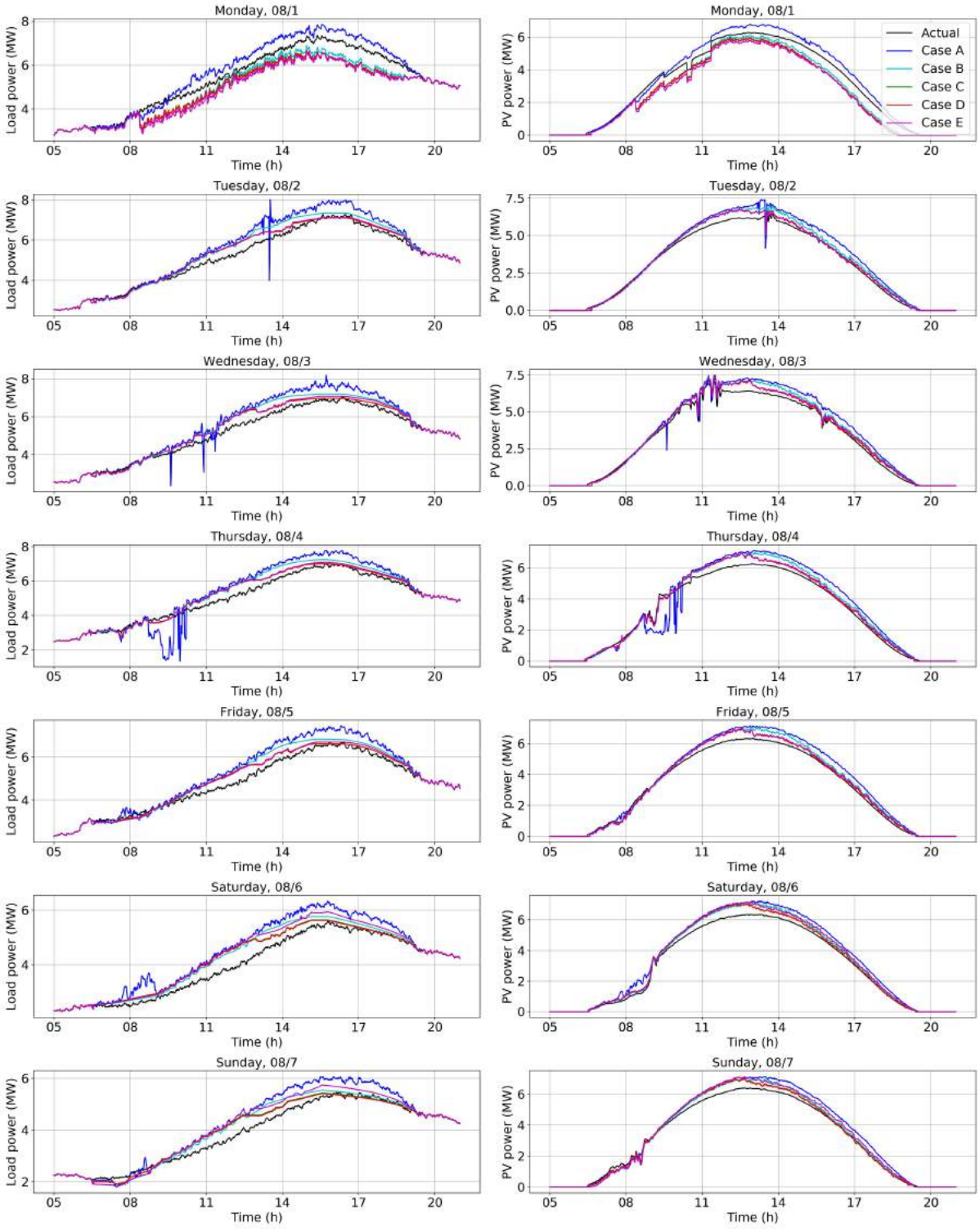

FIG. 14. Actual and disaggregated load power (left plots) and PV power (right plots) for one week in August. Disaggregation results are shown for cases A - E of Table VII.

formance by approximately 50% compared with Kara *et al.* (2018) under the same testing conditions.

G. Benchmarking against a Transposition Model

In order to benchmark the proposed approach against a commonly used transposition model, we use PVLIB (Holm-

TABLE VIII. RMSE for the proposed CSSS-based Case E and a common transposition-based approach.

	January RMSE (kW)	August RMSE (kW)
Case E	199	358
Transposition	890	649

gren, Hansen, and Mikofski, 2018) to simulate the power output for two tilt/azimuth configurations given by the main PV system and the proxy shown in Table I. All other properties are fixed using the Typical Meteorological Year (TMY) data sets from the National Solar Radiation Data Base (Wilcox, 2007) as input. The ratio of the simulated power generation profiles defines the time varying *correction factor*

$$corr_t = \frac{P_{\text{TMY},t}^{\text{tilt=7.5°, azimuth=180°}}}{P_{\text{TMY},t}^{\text{tilt=20°, azimuth=195°}}}. \tag{13}$$

This correction factor time series is then interpolated to 1-minute resolution and used to estimate the active power generation of the unmonitored PV system based on the recorded power output of the PV proxy. The reasoning behind this approach is that $corr_t$ compensates for the differences in tilt/azimuth between our reference system and that we wish to estimate. Therefore, estimation is performed using

$$P_{\text{PV},t} = \eta \; corr_t \; \phi_t, \tag{14}$$

where η is a scaling parameter capturing the different power ratings of the two PV systems. We place no assumptions regarding the capacity of both systems but rather perform a linear regression to determine the optimal value of η, given the transposition corrected proxy measurements, $corr_t \; \phi_t$, as the input and $P_{\text{PV},t} = P_{\text{PMU}_2,t}$ as the output, i.e. the PMU-measured power output of the main system. The RMSE of the transposition approach is then given as the RMSE of this fit. The scaling parameter η was allowed to be different for January and August.

The performance of this transposition model is compared to the CSSS-based Case E disaggregation method in Table VIII. For both months the proposed approach outperforms the transposition-based model with the performance difference larger in January due to the transposition suffering from localized short-term cloud cover in both locations.

H. Effect of Dynamic Power Factor under Volt-Var Control

As the integration of smart PV inverters with advanced control capabilities (such as virtual inertia with grid-forming control or reactive power control for voltage regulation) is expected to increase, it is interesting to investigate the performance of the proposed PV disaggregation method in such a scenario. Specifically, the performance might decrease because the load model in (2) does not account for provision of grid services by the PV systems.

In this paper, we focus on reactive power support in the form of Volt-Var control based on local voltage measurements. We assume that the inverter of the RPU PV system provides reactive power compensation up to 20% of its rated apparent power capacity (i.e. $Q_{\text{max}} = 1500$ kVar), the voltage setpoint is 0.99 p.u., and the Volt-Var deadband is $\pm 0.5\%$. On the contrary, the irradiance proxy PV system does not react to voltage measurements. As a result, the RPU PV operates under a time-varying power factor and thus the scaling ratios between the two PV systems will be affected. In addition, the aggregate reactive power measurements at the feeder head will be distorted and thus the PV disaggregation task will now be harder. Using this setup, we run simulations for August and report the results in Table IX and Fig. 15.

TABLE IX. Comparison of disaggregation RMSE (kW) with and without Volt-Var control in August.

	Disaggregation Case				
Simulation Scenario	A	B	C	D	E
(I). No Volt-Var	508	344	320	334	358
(II). With Volt-Var	518	396	462	399	378
RMSE increase w.r.t. (I) in %	3.5	15.1	44.4	19.5	5.6

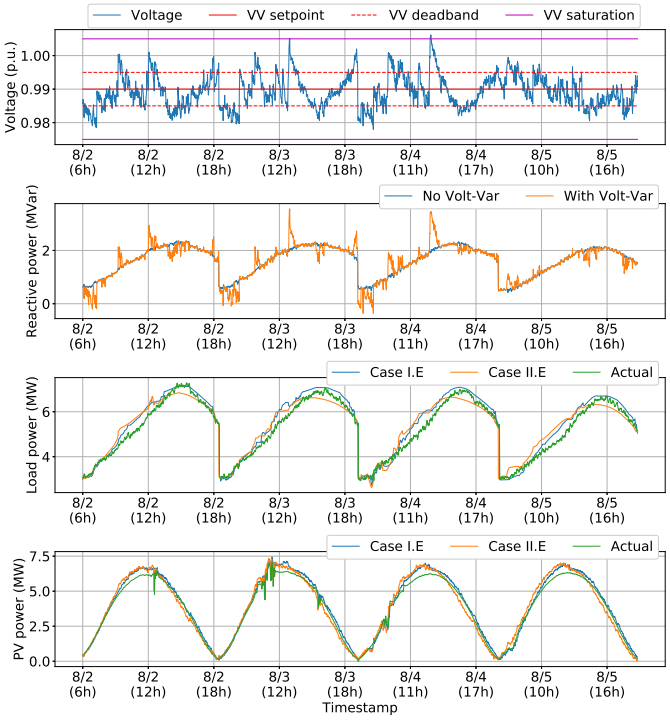

FIG. 15. Simulation results for Case E in August with and without Volt-Var (VV) control from the PV inverter. First plot: Voltage profile and Volt-Var curve parameters. Second plot: Aggregate reactive power at the feeder head. Third plot: Load disaggregation (the legend corresponds to the naming convention of Table IX). Fourth plot: PV disaggregation.

Scenario I in Table IX corresponds to the results of Table VII which are repeated here for convenience, whereas Scenario II assumes that the inverter provides Volt-Var control. As expected, performance degrades under Volt-Var control, especially in Case C. However, note that RMSE increases by

not more than 20% for Cases B and D, and by not more than 6% for Cases A and E. Since Case E is the formulation proposed for implementation, these results indicate that PV disaggregation can also be applied for inverters operating under dynamic power factors. In future work, it would be interesting to investigate potential improvements by adding voltage measurements as an additional regressor in the load demand model of the PV disaggregation problem. This modeling is motivated by the fact that the aggregate reactive power is affected by the inverter's reactive power injection, which in turns depends on the voltage.

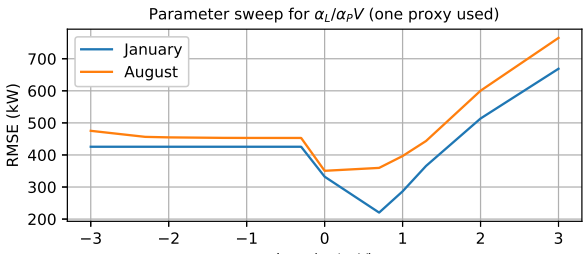

FIG. 16. Dependence of disaggregation RMSE on the $\alpha_{\mathrm{L}}/\alpha_{\mathrm{PV}}$ ratio for the distributed PV system case in January and August.

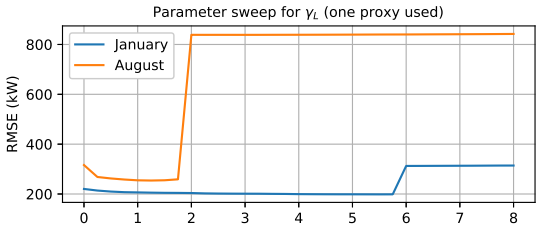

FIG. 17. Dependence of disaggregation RMSE on the γ_{L} factor for the distributed PV system case in January and August.

I. Disaggregation Performance with Distributed PV Systems

1. *Analysis of Weighting Factors and Number of Proxies*

In this section, we present simulation results for the case of distributed PV systems. As a first step, we sweep the weighting factors of CSSS problem for the distributed PV system case to identify how their optimal values compare to those of the single PV system case. To reduce the number of simulations, we apply the load model with ambient temperature and weekday-weekend dependence for all parameter sweeps, use the ℓ_1 norm for the loss function and regularization, and activate the sign constraints (5e), (5f). These settings are motivated by their superior performance in the single PV system case. Furthermore, the analysis is performed with one PV proxy with South-West orientation, i.e. we assume that only one PV system is monitored. We sequentially sweep $\alpha_{\mathrm{L}}/\alpha_{\mathrm{PV}}$, γ_{L}, and β_{PV} and fix the optimal result of each parameter sweep for the next one.

The results are shown in Figs. 16, 17 and 18. The optimal values of $\alpha_{\mathrm{L}}/\alpha_{\mathrm{PV}}$ turn out to be exactly the same as in the single PV system case, i.e. 5 in January and 1 in August. The optimal range for γ_{L} is $4-5.75$ in January and $1-1.5$ in August, which are close to the respective ranges for the single PV system case. As far as the time-varying regressors are concerned, RMSE is much less sensitive to the number of time windows and the β_{PV} factors compared with the results of Fig. 12. In January, exactly the same optimal parameterization with the centralized PV case is obtained (2 windows and $\beta = 0$), and the minimum disaggregation RMSE is 197 kW, i.e. practically the same with that of the centralized case (Table VI). In August, 3 windows and $\beta = 10^6$ are optimal; however, note that the parameterization from the centralized case (2 windows and $\beta = 10^4$) also improves performance compared with using no time windows. Interestingly, the minimum disaggregation RMSE in August is 234 kW, which is significantly lower than that of the centralized PV case (Table VII).

In a second step, we investigate how disaggregation performance depends on the number of irradiance proxies, i.e. on the number of monitored PV systems. Note that, besides the total number of proxies, their orientation is also an important factor and it follows the distribution shown in Table II. Out of the $N_{\mathrm{orient}} = 6$ possible orientations, the dominant one is South-West, followed by South and West orientations, whereas there are only a few PV stations with other orientations. Intuitively, one would expect that disaggregation performance improves if: (i) the PV systems used as proxies reflect the distribution of orientations from Table II; and (ii) all possible orientations are included in the set of proxies. For this purpose, we use the following sequential approach to select the PV systems that will be used as proxies for each simulated case of total number of proxies ($N_{\mathrm{p},j}$):

- If $N_{\mathrm{p},j} \leq N_{\mathrm{orient}}$, then we select $N_{\mathrm{p},j}$ PV systems with different orientations following the descending order of Table II.
- If $N_{\mathrm{p},j} > N_{\mathrm{orient}}$, then the set of proxies contains the $j-1$ PV systems already selected for the previous case (number of proxies equal to $N_{\mathrm{p},j-1}$), as well as a new PV system that is randomly sampled from the discrete probability distribution of Table II.

The simulation results are shown in Fig. 19 for January and August. In January, cases B - E considerably outperform the base Case A for any percentage of monitored PV systems. In August, however, the situation is different. Cases D and E perform better than Case A up to an approximately 15% percentage of monitored PV systems, whereas Case A is best afterwards. With the exception of using only one proxy, Cases B and C are worse than Case A. Furthermore, note that using only 1 or 2 proxies gives the best results for both months. This might be counter-intuitive, as one would expect the disaggregation error to generally decrease with more irradiance proxies. However, recall that the first and second proxies are PV systems with South-West and South orientations, respectively, which collectively represent the orientations of 83% of all PV systems. Therefore, a few proxies are sufficient to estimate the total PV power, whereas using additional proxies weighs

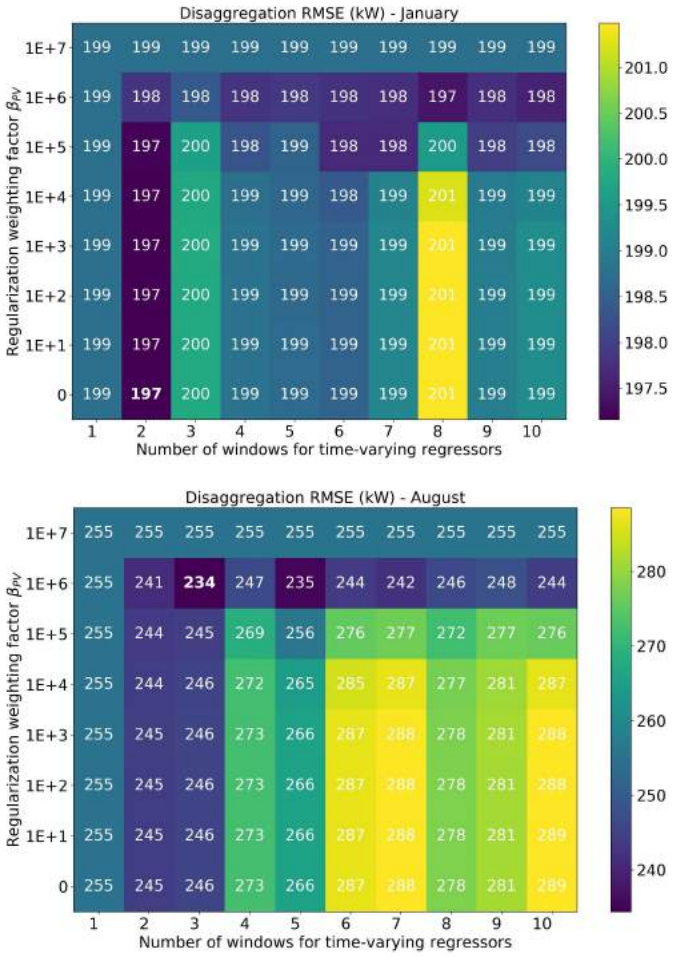

FIG. 18. Distributed PV system case: disaggregation performance for different combinations of time windows and regularization factors for solar power in January (top) and August (bottom).

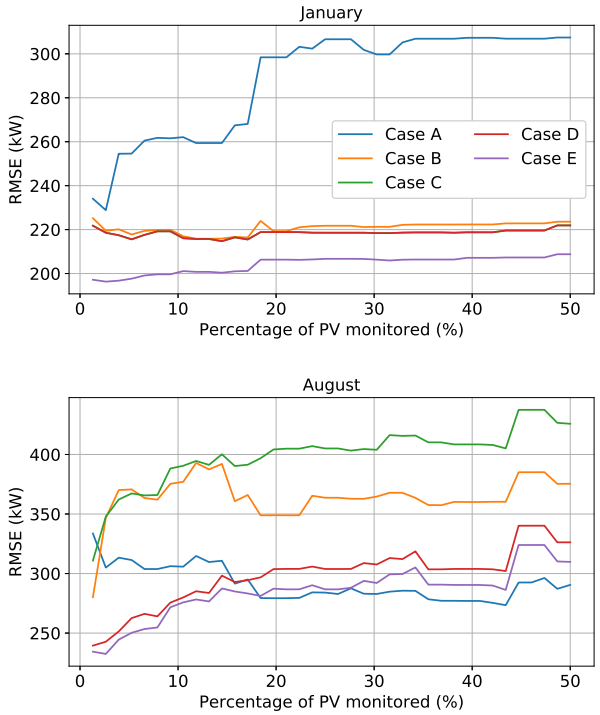

FIG. 19. Disaggregation results as a percentage of monitored PV systems for cases A - E for January (top) and August (bottom).

disproportionately uncommon orientations and consequently distorts the predictions.

2. *Practical Aspects of Weighing Factor Tuning*

Overall, our results show that the developed PV disaggregation method works also for distributed PV systems and that the disaggregation performance is similar, or even higher, compared with the single PV system case. In particular, the optimal weighting factors are generally similar in the centralized and distributed PV system cases. As mentioned in Section II D, tuning of weighting factors requires access to aggregated PV generation profiles of specific feeders. Obtaining power generation profiles for all PV installations, however, may be impractical. Alternatively, a subset of profiles can be used, with appropriate geographic smoothing (Marcos *et al.*, 2011; Lave, Kleissl, and Stein, 2013), and scaled up to the total installed capacity for weight-tuning purposes.

Our results indicate that the optimal weighting factors will be different for each season or even each month. In addition, since PV disaggregation is formulated as a multi-objective optimization problem and the weighting factors are optimized for a base-case system setup, disaggregation performance might degrade if the same weighting factors are used for significantly different system setups. Changes in system setup include increase or decrease of total installed PV power and/or number of distributed PV systems, changes in tilt or orientation of some PV systems, growth or reduction of load demand, etc. Nevertheless, if the algorithm is insensitive to such system changes, it would still be possible to come up with optimal weighting factors for each month of the year that are updated infrequently, e.g., on an annual basis. We restrict our attention to algorithm's sensitivity to the total installed PV power, which we vary in the range $[-70\%, +100\%]$ of the base case, i.e. the total installed PV power in our dataset. We then simulate using the CSSS algorithm for Case E with only one proxy, as this combination achieves very good performance both in January and August.

The simulation results are presented in Fig. 20. In January, the absolute RMSE increases only marginally for PV power larger or smaller than the base case. In August, the absolute RMSE consistently increases with the PV power. In both months, the relative RMSE decreases for PV power larger than the base case. Note that if the PV power changes within $\pm 25\%$ of the base case, the relative RMSE remains within $\pm 1.25\%$ of the base case's RMSE. These results show that the disaggregation performance is rather insensitive to the total installed PV power. Therefore, this is an indication that it

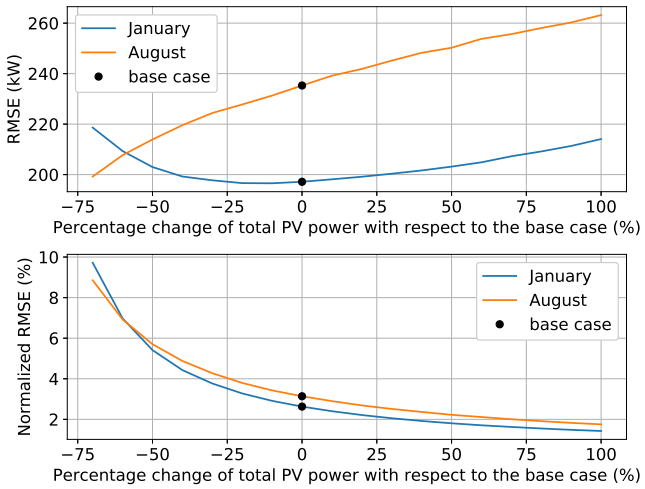

FIG. 20. Sensitivity of disaggregation error to total PV power for Case E using only one irradiance proxy. Top: absolute RMSE. Bottom: RMSE normalized with total installed PV power.

would suffice to optimize the weighting factors infrequently, e.g., on an annual basis.

V. CONCLUSION

In this paper, we presented a method to disaggregate PV power from aggregate active and reactive power measurements (e.g., from PMUs connected at the substation or feeder head). The method also relies on active power measurements from one or a few nearby monitored PV systems that are used as irradiance proxies and, in some cases, measurements of ambient temperature. The disaggregation was formulated as a multi-objective optimization problem, which minimizes prediction error of linear regression models and integrates regularization terms for time-varying regressors and the estimated PV and load source signals. The paper also presented a thorough parametric analysis to identify optimal values for the associated weighting factors in the objective function, as well as their seasonal dependence. Simulation results showed that the method provides accurate estimates of PV power for both the centralized and distributed PV cases. Specifically, RMSE is 3.5% on average (normalized by installed PV power), which is 50% lower than that of earlier work Kara *et al.* (2018). In the following, we summarize the most important recommendations for practical implementation based on the findings of our analyses.

- Using the ℓ_1 norm for both loss function and regularization terms was shown to give better results than the ℓ_2 norm.
- The best practice is to apply source regularization only for the load signal, and use time-varying regressors and regressor regularization only for the PV signal. Capturing the weekday/weekend dependence of load as well as its dependence on ambient temperature is recommended.
- The weighting factors in the objective function are seasonal and should be tuned separately for each month. However, our results indicate that it suffices to perform tuning infrequently (e.g., on an annual basis) because the algorithm is not very sensitive to changes in installed PV power.
- Adding sign constraints for the source signals and regressors was shown to reduce the risk of overfitting and improve robustness of results.
- For the distributed PV case, it is preferable to use as irradiance proxies only a few (one or two) monitored PV systems, which represent the most common orientations in the group of PVs.

Future work can focus on demonstrating the algorithm on larger data sets that include shoulder months in fall and spring. In addition, the temperature-dependent load model can be improved by introducing a shifting matrix, or by using a piecewise linear model as in Tabone, Kiliccote, and Kara (2018); Mathieu *et al.* (2011), to account for the fact that temperature typically affects load demand with some delay. Furthermore, it would be interesting to investigate the necessity of using an averaging filter for the irradiance proxies in case of distributed PV systems, and quantify the effect of the averaging period on the algorithm's performance. Even though the results for the single PV system suggest that the method works also with time-varying power factors, additional work is needed to investigate its performance for distributed PV systems with large variability in power factor due to smart inverter operation for voltage control. Finally, further analysis of the algorithm's sensitivity to additional system changes, such as the peak load demand, will help determine more specific requirements on how often the weighting factors need to be tuned.

VI. ACKNOWLEDGEMENTS

The authors would like to thank Riverside Public Utilities (RPU) and UCR for the data used in this study, and Prof. Jan Kleissl from the University of California at San Diego for constructive feedback and suggestions to improve the manuscript. This work was partially funded by U.S. Department of Energy's Advanced Research Projects Agency-Energy (ARPA-E). Lawrence Berkeley National Laboratory is operated for the US Department of Energy by the University of California under Contract No. DE-AC02-05CH11231.

Bright, J. M., Killinger, S., Lingfors, D., and Engerer, N. A., "Improved satellite-derived PV power nowcasting using real-time power data from reference PV systems," Solar Energy **168**, 118–139 (2018).

Chen, D. and Irwin, D., "Sundance: Black-box behind-the-meter solar disaggregation," in *Proceedings of the Eighth International Conference on Future Energy Systems* (ACM, 2017) pp. 45–55.

Diamond, S. and Boyd, S., "CVXPY: A Python-embedded modeling language for convex optimization," Journal of Machine Learning Research **17**, 1–5 (2016).

Dinesh, C., Welikala, S., Liyanage, Y., Ekanayake, M. P. B., Godaliyadda, R. I., and Ekanayake, J., "Non-intrusive load monitoring under residential solar power influx," Applied Energy **205**, 1068–1080 (2017).

Gueymard, C. A., "Progress in direct irradiance modeling and validation," in *Solar 2010 Conf., Phoenix, AZ, American Solar Energy Society* (2010).

Holmgren, W. F., Hansen, C. W., and Mikofski, M. A., "pvlib python: a python package for modeling solar energy systems," The Journal of Open Source Software **3**, 884 (2018).

Kara, E. C., Roberts, C. M., Tabone, M., Alvarez, L., Callaway, D. S., and Stewart, E. M., "Disaggregating solar generation from feeder-level measurements," Sustainable Energy, Grids and Networks **13**, 112–121 (2018).

Kara, E. C., Tabone, M., Roberts, C., Kiliccote, S., and Stewart, E. M., "Estimating behind-the-meter solar generation with existing measurement infrastructure," in *Proceedings of the 3rd ACM International Conference on Systems for Energy-Efficient Built Environments* (ACM, 2016) pp. 259–260.

Keogh, E. and Ratanamahatana, C. A., "Exact indexing of dynamic time warping," Knowledge and information systems **7**, 358–386 (2005).

Killinger, S., Braam, F., Müller, B., Wille-Haussmann, B., and McKenna, R., "Projection of power generation between differently-oriented PV systems," Solar Energy **136**, 153–165 (2016).

Lave, M., Hayes, W., Pohl, A., and Hansen, C. W., "Evaluation of global horizontal irradiance to plane-of-array irradiance models at locations across the United States," IEEE journal of Photovoltaics **5**, 597–606 (2015).

Lave, M., Kleissl, J., and Stein, J. S., "A wavelet-based variability model (WVM) for solar PV power plants," IEEE Transactions on Sustainable Energy **4**, 501–509 (2013).

Marcos, J., Marroyo, L., Lorenzo, E., Alvira, D., and Izco, E., "From irradiance to output power fluctuations: the PV plant as a low pass filter," Progress in Photovoltaics: Research and Applications **19**, 505–510 (2011).

Mathieu, J. L., Price, P. N., Kiliccote, S., and Piette, M. A., "Quantifying changes in building electricity use, with application to demand response," IEEE Transactions on Smart Grid **2**, 507–518 (2011).

Mehmood, K. K., Khan, S. U., Lee, S.-J., Haider, Z. M., Rafique, M. K., and Kim, C.-H., "A real-time optimal coordination scheme for the voltage regulation of a distribution network including an OLTC, capacitor banks, and multiple distributed energy resources," International Journal of Electrical Power & Energy Systems **94**, 1–14 (2018).

Mills, A. and Wiser, R., "Implications of wide-area geographic diversity for short-term variability of solar power," Tech. Rep. (Lawrence Berkeley National Lab.(LBNL), Berkeley, CA (United States), 2010).

Palmintier, B., Broderick, R., Mather, B., Coddington, M., Baker, K., Ding, F., Reno, M., Lave, M., and Bharatkumar, A., "On the path to SunShot. Emerging issues and challenges in integrating solar with the distribution system," Tech. Rep. (National Renewable Energy Lab. (NREL), Golden, CO (United States), 2016).

Pierro, M., De Felice, M., Maggioni, E., Moser, D., Perotto, A., Spada, F., and Cornaro, C., "Data-driven upscaling methods for regional photovoltaic power estimation and forecast using satellite and numerical weather prediction data," Solar Energy **158**, 1026–1038 (2017).

Ruf, H. I., *Computation of the load flow at the transformer in distribution grids with a significant number of photovoltaic systems using satellite-derived solar irradiance data*, Ph.D. thesis, University of Agder, Norway (2016).

Shaker, H., Zareipour, H., and Wood, D., "A data-driven approach for estimating the power generation of invisible solar sites." IEEE Trans. Smart Grid **7**, 2466–2476 (2016a).

Shaker, H., Zareipour, H., and Wood, D., "Estimating power generation of invisible solar sites using publicly available data," IEEE Transactions on Smart Grid **7**, 2456–2465 (2016b).

Sossan, F., Nespoli, L., Medici, V., and Paolone, M., "Unsupervised disaggregation of photovoltaic production from composite power flow measurements of heterogeneous prosumers," IEEE Transactions on Industrial Informatics (2018).

Tabone, M., Kiliccote, S., and Kara, E. C., "Disaggregating solar generation behind individual meters in real time," in *Proceedings of the BuildSys Conference* (ACM, November 2018).

Taylor, Z., Akhavan-Hejazi, H., Cortez, E., Alvarez, L., Ula, S., Barth, M., and Mohsenian-Rad, H., "Battery-assisted distribution feeder peak load reduction: Stochastic optimization and utility-scale implementation," in *Power and Energy Society General Meeting (PESGM), 2016* (IEEE, 2016) pp. 1–5.

Wang, Y., Zhang, N., Chen, Q., Kirschen, D. S., Li, P., and Xia, Q., "Data-driven probabilistic net load forecasting with high penetration of behind-the-meter pv," IEEE Transactions on Power Systems **33**, 3255–3264 (2018).

Wilcox, S., "National solar radiation database 1991-2005 update: User's manual," Tech. Rep. (National Renewable Energy Lab. (NREL), Golden, CO (United States), 2007).

Wytock, M. and Kolter, J. Z., "Contextually supervised source separation with application to energy disaggregation." in *AAAI Conference on Artificial Intelligence* (2014) pp. 486–492.